UNIVERSITY OF HELSINKI REPORT SERIES IN PHYSICS

HU-P-D91

FINAL-STATE INTERACTIONS IN INELASTIC X-RAY SCATTERING

Aleksi Soininen

X-Ray Laboratory
Department of Physics
Faculty of Science
University of Helsinki
Helsinki, Finland

ACADEMIC DISSERTATION

To be presented, with the permission of
the Faculty of Science of the University of Helsinki,
for public criticism in Auditorium E204 of
the Department of Physics on July 18th, 2001, at 12 o'clock noon.

Helsinki 2001

ISBN 951-45-8948-3
ISBN 952-10-0016-3 (pdf versio)
ISSN 0356-0961
Tummavuoren Kirjapaino
Vantaa 2001

Preface

This thesis is based on research done at the X-ray Laboratory of the Department of Physics (University of Helsinki, Finland) and at the National Institute of Standards and Technology (Maryland, USA).

I would like to thank Prof. Seppo Manninen and Docent Keijo Hämäläinen for introducing me to the field of non-resonant inelastic x-ray scattering. Additionally, I would like to thank them for the guidance and encouragement they have given me throughout this work. I would like to express my gratitude to Dr. Eric Shirley whose contribution to this work was invaluable. I would also like to express my gratitude to the late Prof. Teijo Åberg for the guidance he gave me in the early stage of this work.

I would like to acknowledge the staff of the X-ray Laboratory of the University of Helsinki for creating a good working environment. The lively discussions at the laboratory coffee table are fondly remembered. Especially I would like to thank Dr. Jarkko Laukkanen, M.Sc. Simo Huotari, and M.Sc. Szabolcs Galambosi.

I am grateful to Prof. Juhani Keinonen for giving me the opportunity to work at the Department of Physics.

I would like to thank the inelastic X-ray scattering group at the University of Dortmund for their hospitality during my stays in Dortmund. Especially I would like to thank Prof. Winfried Schülke, Dr. Christian Sternemann, Gordon Döring, and Hartmut Enkisch for helpful discussions. I would also like to thank Dr. Bernardo Barbiellini for the help he gave me in the early stages of the *GW* spectral function project.

The financial support of the Academy of Finland and the Finnish Academy of Science and Letters is gratefully acknowledged.

Helsinki, 7^{th} of June 2001

Aleksi Soininen

J. A. Soininen: Final-State Interactions in Inelastic X-ray Scattering, University of Helsinki (2001), 37 pages + Appendices, University of Helsinki, Report Series in Physics, HU-P-D91, ISSN 0356-0961, ISBN 951-45-8948-3.

Classification (INSPEC): A7870C, A7110, A7130, A7145G
Keywords: inelastic x-ray scattering, final-state interactions, computational methods

Abstract

The development of new synchrotron x-ray sources has significantly increased the use of x-rays in the characterization of solids. The need to understand and analyze these results has partly motivated the development of new computational methods that can reliably handle excited states of solids. Although many of these methods aim to be independent of the experimental results, they often include approximations that can only be justified by how well they can predict the experimental results. This is why a collaboration of the experimental, theoretical and computational efforts is important for the development of these methods.

This work introduces computational methods and approximations that can be used to study the excited states of electrons produced by non-resonant inelastic x-ray scattering. First an *ab initio* scheme to calculate the dielectric function for finite momentum transfers is introduced. It is used to analyze the results of non-resonant inelastic x-ray scattering from valence electrons of several semiconductor materials. The scheme is found to correctly predict the inelastic x-ray scattering spectra in different types of semiconductors. Furthermore, another scheme is introduced for calculating core-excited states in solids and it is applied to a wide range of materials. Although this scheme is based on the same theoretical formalism as the work on the valence-excited states, some modifications were made to correctly treat core excitations. Again, by comparing the calculated results with the experimental ones the scheme is found to work well. Additionally, the effects of the final-state electron-electron correlations on the high-energy and momentum transfer inelastic x-ray scattering are studied using a model spectral function developed in this work. These results are used to discuss the validity of the impulse approximation in light of the final-state electron-electron interaction. These final-state correlations were found to explain some previously unresolved differences between experiments and theoretical calculations.

Contents

List of papers

This thesis consists of an introductory part followed by five research papers.

I J. A. Soininen and Eric L. Shirley, *Effect of electron-hole interaction on the dynamic structure factor: Application to nonresonant inelastic x-ray scattering*, Phys. Rev. B **61**, 16423 (2000).

II E. L. Shirley, **J. A. Soininen**, G. P. Zhang, J. A. Carlisle, T. A. Callcott, D. L. Ederer, L. J. Terminello, and R. C. C. Perera, *Modeling final-state interaction effects in inelastic x-ray scattering from solids: resonant and non-resonant*, J. El. Spect. and Rel. Phenom. **114-116**, 939 (2001).

III J. A. Soininen and Eric L. Shirley, *A scheme to calculate core hole-electron interactions in solids*, submitted for publication to Phys. Rev. B.

IV J. A. Soininen, W. Caliebe, C.-C. Kao, Eric L. Shirley, and K. Hämäläinen, *Core hole-electron Interaction in x-ray Raman scattering*, submitted for publication to J. Phys: Condens. Matter.

V J. A. Soininen, K. Hämäläinen, and S. Manninen, *Final state electron-electron interaction in Compton scattering*, submitted for publication to Phys. Rev. B.

The author of this thesis is responsible for the theoretical work, the code development and the computational work in these papers when it is used to study non-resonant inelastic scattering. The author of this thesis is the principal author in all of the papers except for the paper II where he is a contributing author.

1 Introduction

The first to correctly interpret inelastic x-ray scattering experiments were Compton [1] and Debye [2]. They used, at the time, a new and controversial concept of the light quantum to explain the experimental results. Only few years after this discovery DuMond [3] measured the Compton profile of beryllium metal and was able to show that the conduction electrons obeyed the Fermi-Dirac distribution. After this early work the experimental development in inelastic x-ray scattering has been rather independent of the advances in the theoretical understanding of the electron systems. However, often enough the theoretical ideas and models have been tested by comparing them to inelastic x-ray scattering results.

Inelastic x-ray scattering can be used to probe different physical properties of solids. Since a solid is a true many-particle system, the use of many-body formalism is unavoidable in any theoretical study of inelastic x-ray scattering from solids. The x-rays scatter mostly from the electrons and the properties of electrons in their ground or excited state determines the scattering cross sections of most hard[1] x-ray scattering experiments. The theoretical formalism used in the modern studies of many-electron systems was, for the most part, developed early in the second half of the 20th century. The subsequent work has concentrated on the development of practical approximations for dealing with the many-electron systems found in nature, such as solids.

The development of the 3rd-generation synchrotron x-ray sources has radically changed the use of x-ray scattering in materials science [4]. The properties of the synchrotron radiation, such as tunable photon polarization and energy combined with high intensity and natural collimation, have made possible experiments that were infeasible using the conventional x-ray sources. In inelastic x-ray scattering the tunability of the incident energy made it feasible to study high-Z materials using resonant inelastic x-ray scattering [5, 6]. Synchrotron radiation has also made it possible to study previously discovered phenomena in more detail. By studying the momentum-transfer dependence of the spectral features the dispersion or even the symmetry of the corresponding excitations can be determined. In the high momentum transfer limit, i.e., in the limit where the impulse approximation [7] is valid, inelastic scattering can be used to study the ground-state momentum density of a system. With the new synchrotron sources a wide range of properties of materials can be studied using inelastic x-ray scattering.

The new experimental results in inelastic x-ray scattering have challenged the theoretical understanding of the properties of electrons in solids. Even in relatively simple systems, such as metals, the experimental results have eluded complete theoretical explanation. For example, the Compton profile and discontinuity (Z_f) of

[1] Hard x-rays have energy over few keV

the momentum distribution function at the Fermi break has been measured for several metals (see for example [8–10]). In lithium (Li) the Z_f estimated from experiments [9, 10] disagreed with the earlier theoretical estimates. This motivated several theoretical studies [11–16] which disagreed not only on the origin of the experimental results but also on their estimates on the value of Z_f. Also the general shape and dispersion of the dynamic structure factor has attracted both experimental and theoretical interest [17–19]. The experimental results for the local-field factor disagree with the earlier theoretical predictions in the moderate-momentum-transfer regime [19]. These studies are examples of how new inelastic x-ray scattering results have raised questions about widely used theoretical approximations.

This work presents computational methods which can be used to study excited electron states in solids and their applications to non-resonant inelastic x-ray scattering. Reliable computational schemes for describing the ground-state properties of solids have existed for several years. Only in more complex systems, such as strongly correlated systems or systems with crystal defects, does the ground-state evade complete theoretical understanding. The excited states have proven to be harder to treat with the same accuracy. This is why, even today, the theoretical approaches used in the analysis of inelastic x-ray scattering are often based on a single-particle approximation. The final state and many-particle interactions of the electron system are either neglected or they are included using phenomenological corrections. Only during the recent years there have been advances both in the algorithms and the computational power that have made it possible to treat the excited states more accurately.

This summary starts with a short review of the non-resonant inelastic x-ray scattering. Next the theoretical approaches and the approximations used in this work are introduced on a general level. A more detailed discussion on the different applications of these approximations follows. Some previously unpublished details of the work are also discussed. Examples of the computational schemes applied to different materials are given in this summary and more examples can be found in the included papers.

2 Non-resonant Inelastic X-ray Scattering

In this section the theoretical basis of non-resonant inelastic x-ray scattering is presented. The scattering cross section is derived starting from the non-relativistic expression for the electron-photon interaction. Also the general properties of the cross-section are discussed.

2.1 Interaction Hamiltonian and the Cross Section

In the presence of an electromagnetic field the Hamiltonian of the combined electron-photon system can be written with three terms:

$$\mathbf{H} = \mathbf{H}_e + \mathbf{H}_p + \mathbf{H}_{e-p},$$

where $\mathbf{H}_e$ is the Hamiltonian of the electrons in the absence of the external field, $\mathbf{H}_p$ is the photon field Hamiltonian, and the last term $\mathbf{H}_{e-p}$ represents the interaction between the electrons and the photon field. In the non-relativistic limit the interaction Hamiltonian $\mathbf{H}_{e-p}$ is

$$\mathbf{H}_{e-p} = \sum_i (\frac{\alpha^2}{2}\mathbf{A}_i \cdot \mathbf{A}_i + \alpha \mathbf{p}_i \cdot \mathbf{A}_i), \tag{1}$$

where $\mathbf{A}_i$ is the vector field operator, $\mathbf{p}_i$ is the electron momentum operator and α is the fine structure constant. The sum is over the electrons (i) in the system. The vector field is assumed to follow the Coulomb gauge (i.e. $\nabla_i \cdot \mathbf{A}_i = 0$), and in the Heisenberg representation it can be written in a quantized form as

$$\mathbf{A}_i(t) = \sum_{\mathbf{k},\eta} (\frac{2\pi}{V\omega_\mathbf{k}\alpha^2})^{1/2} \left[\hat{a}_{\mathbf{k}\eta}\boldsymbol{\varepsilon}_\eta e^{i(\mathbf{k}\cdot\mathbf{r}_i - \omega_\mathbf{k} t)} + \hat{a}^\dagger_{\mathbf{k}\eta}\boldsymbol{\varepsilon}^*_\eta e^{-i(\mathbf{k}\cdot\mathbf{r}_i - \omega_\mathbf{k} t)}\right], \tag{2}$$

where the photons are characterized by their momentum $\mathbf{k}$ and their polarization state η (with polarization vector $\boldsymbol{\varepsilon}_\eta$). The quantization has been done in a volume V and $\hat{a}^\dagger$ ($\hat{a}$) is the photon creation (annihilation) operator.

In first-order perturbation theory the first term of Eq. (1) represents scattering (elastic or inelastic) and the second term absorption and emission. In an x-ray scattering process there is one photon in the initial and in the final state. The scattering cross section for such a process is given in the second order by the Kramers-Heisenberg formula:

$$\begin{aligned}
\frac{d^2\sigma}{d\Omega d\omega_2} &= r_0^2 \frac{\omega_2}{\omega_1} \sum_F |\langle F| \sum_i e^{i(\mathbf{k}_1 - \mathbf{k}_2)\cdot\mathbf{r}_i} |I\rangle (\boldsymbol{\varepsilon}_1 \cdot \boldsymbol{\varepsilon}_2^*) \\
&- \sum_M [\frac{\langle F| \sum_i (\boldsymbol{\varepsilon}_1 \cdot \mathbf{p}_i) e^{i\mathbf{k}_1\cdot\mathbf{r}_i} |M\rangle\langle M| \sum_i (\boldsymbol{\varepsilon}_2^* \cdot \mathbf{p}_i) e^{-i\mathbf{k}_2\cdot\mathbf{r}_i} |I\rangle}{E_M + \omega_2 - E_I} \\
&+ \frac{\langle F| \sum_i (\boldsymbol{\varepsilon}_2^* \cdot \mathbf{p}_i) e^{-i\mathbf{k}_2\cdot\mathbf{r}_i} |M\rangle\langle M| \sum_i (\boldsymbol{\varepsilon}_1 \cdot \mathbf{p}_i) e^{i\mathbf{k}_1\cdot\mathbf{r}_i} |I\rangle}{E_M - \omega_1 - E_I - i\Gamma_M}]|^2 \\
&\times \delta(\omega_1 - \omega_2 + E_I - E_F).
\end{aligned} \tag{3}$$

Here the initial (final) photon momentum, energy and polarization vector are given by $\mathbf{k}_1$, ω_1 and ε_1 ($\mathbf{k}_2$, ω_2 and ε_2) respectively. The three states I, M and F denote the initial, intermediate and final states of the electrons and their energies are given by E_I, E_M and E_F. Γ_M is the inverse of the intermediate-state lifetime. The third term in Eq. (3) is resonant and gives a strong contribution if the energy of the incoming

photon (ω_1) is tuned close to an x-ray absorption edge. If the incident photon energy is far away from the x-ray edges, the non-resonant first term dominates. In this case the cross section can be given in a simple form

$$\frac{d^2\sigma}{d\Omega d\omega_2} = \left(\frac{d\sigma}{d\Omega}\right)_{Th} S(\mathbf{q},\omega), \tag{4}$$

where $S(\mathbf{q},\omega)$ is the dynamic structure factor (DSF)

$$S(\mathbf{q},\omega) = \sum_F |\langle F| \sum_i e^{i\mathbf{q}\cdot\mathbf{r}_i} |I\rangle|^2 \, \delta(\omega + E_I - E_F) \tag{5}$$

and $(d\sigma/d\Omega)_{Th}$ is the Thomson scattering cross section.[2] The dynamic structure factor depends on the momentum transfer $\mathbf{q} = \mathbf{k}_1 - \mathbf{k}_2$ and energy transfer $\omega = \omega_1 - \omega_2$ from the photon to the electron system and on the properties of the excited states of the system. The Thomson cross section represents the electron-photon coupling. In other words, in the expression for the cross section the information about the studied system and the probe is separated. In fact, the cross section for electron energy loss spectroscopy (EELS) can be approximated with a similar equation except that $(d\sigma/d\Omega)_{Th}$ is replaced with an appropriate cross section for electron-electron scattering.

2.2 Dynamic Structure Factor

As indicated in the previous section the non-resonant inelastic x-ray scattering (NRIXS) cross section is proportional to the dynamic structure factor $S(\mathbf{q},\omega)$. In NRIXS the freedom of choosing the momentum and the energy transfer independently of each other makes it possible to study the properties, such as dispersion, of different types of excitations. The DSF can be represented as a Fourier transform with respect to the time and the position coordinates of the density-density correlation function [22]

$$S(\mathbf{q},\omega) = \frac{1}{2\pi} \int\int\int d\mathbf{r}' \, d\mathbf{r} \, dt \, \langle \rho(\mathbf{r}' - \mathbf{r}, t) \rho(\mathbf{r}', 0) \rangle \, e^{i\mathbf{q}\cdot\mathbf{r}} \, e^{-i\omega t}, \tag{6}$$

where $\rho(\mathbf{r},t)$ is the electron density operator. The expectation value $\langle\rangle$ is taken with respect to the ground state of the system. It can be seen from the Eq. (6) that the magnitude of the momentum transfer $q = |\mathbf{q}|$ and the energy transfer ω determine the spatial and time scales on which the density-density correlations are studied [21]. When the momentum transfer is small compared to the inverse of the characteristic length scale r_c of the system (i.e. for example the average inter-particle distance) the effects of correlations between particles determine the spectrum. For ω close to a typical phonon or plasmon energy the dynamics of these collective excitations can

[2] Following Ref. [21] the factor of ω_2/ω_1 is included into the definition of $(d\sigma/d\Omega)_{Th}$.

be studied in this low-momentum-transfer regime. When the momentum transfer is increased the correlations between particles become less important and in the high-momentum-transfer regime the scattering can be assumed to happen from single particles. However, this simple division is complicated by the many-particle nature of solids. For example, in Cs the plasmon has a negative dispersion at low momentum transfers which was explained by a *first-principles* study of Fleszar et al. [20] to have its origin in the interplay of the low-momentum plasmon with the one-electron excitations. On the other hand, in the high-momentum-transfer region the dynamic structure factor is affected by the fact that the excited particle can decay by coupling to the collective excitations [10].

The dynamic structure factor can also be related to the macroscopic response of the system. This is done by using *fluctuation-dissipation* theorem which relates DSF to the dielectric function $\varepsilon_M(\mathbf{q},\omega)$ of the system

$$S(\mathbf{q},\omega) = -\frac{q^2}{4\pi^2 n}\mathrm{Im}\left[\frac{1}{\varepsilon_M(\mathbf{q},\omega)}\right]. \tag{7}$$

Here ε_M represents the response of the system to the total macroscopic field and n is the average electron density of the system. This relation links the correlations of the system (as given in Eq. (6)) to the dissipation of energy from an external source in the system (as given by $-\mathrm{Im}\,(1/\varepsilon_M)$). In this work the fluctuation-dissipation theorem is used to study valence excitations in section 4 by computing ε_M instead of the dynamic structure factor.

3 Theoretical Background

In this section an overview of the theoretical background of this work is given. The aim is to give a review of the problem and the approximations used in this work. The first subsection is dedicated to the discussion on the general properties of the dynamic structure factor in light of a single- or independent-particle picture. In a single-particle picture the initial and the final state of the electron are calculated using a average ground-state potential due to the other electrons and the nuclei. The effects going beyond this simple approach are commonly called *final-state effects* in different spectroscopies. These include the effects of the interaction of the excited electron (or hole) with its own polarization cloud (i.e., the polarization of the other electrons in the system). These are covered in the second subsection where the single-particle Green's functions are introduced. The interaction between the final-state electron and hole is discussed in the last subsection in which the theory and computation of the two-particle Green's functions are presented.

3.1 Single-Particle Theory

In the single-particle picture the initial and final states in Eq. (5) are replaced by Slater determinants created from single-particle states. This gives a rather simple formula for DSF:

$$S(\mathbf{q},\omega) = \sum_{i}^{occ} \sum_{f}^{unocc} |\langle f|e^{i\mathbf{q}\cdot\mathbf{r}}|i\rangle|^2 \, \delta(\omega + \varepsilon_i - \varepsilon_f), \tag{8}$$

where $|i\rangle$ ($|f\rangle$) denotes the single-particle initial (final) state and ε_i (ε_f) its energy. This expression neglects all the interactions of the final-state hole and the final-state electron that are not included in the single-particle Hamiltonian (H_0). However, it can be used to study the main features of the NRIXS spectra. Also, it enables one to rather easily derive many of the general trends of DSF. For example, in the low momentum transfer limit the exponential in Eq. (8) can be expanded as

$$e^{i\mathbf{q}\cdot\mathbf{r}} = 1 + i\mathbf{q}\cdot\mathbf{r} - (\mathbf{q}\cdot\mathbf{r})^2/2 + \ldots. \tag{9}$$

When this expansion is inserted into Eq. (8) the first term to contribute is proportional to $\mathbf{q}\cdot\mathbf{r}$ and it gives rise to dipole-allowed transitions. When the momentum transfer is increased the other terms and excitation channels (monopole, quadrupole) become more important. In this way the large momentum-transfer range available in NRIXS can be used to study excitations with different symmetries. In the other limit as $q \to \infty$ and $\omega \to \infty$ the expression (8) reduces to the so-called impulse approximation (IA)

$$S(\mathbf{q},\omega) \approx \int d\mathbf{p}\, \rho(\mathbf{p})\, \delta(\omega - \mathbf{p}\cdot\mathbf{q} - q^2/2). \tag{10}$$

Here $\rho(\mathbf{p})$ is the ground-state electron momentum density of the system. The delta function in this equation represents both the energy and the momentum conservation. From this it is easy to understand how the spectrum evolves as the momentum transfer is changed. The term $q^2/2$ determines the position of the peak of the spectrum and $\mathbf{p}\cdot\mathbf{q}$ on the other hand controls the width of the spectra.[3] Although these general trends of the dynamic structure factor were here derived from rather simple approximations, they persist even if more elaborate methods are used.

In this subsection so far we have concentrated on the single-particle excitations in solids. The other important electron excitations that can be studied using NRIXS are plasmons, i.e., collective oscillations of the electrons. To study plasmons we use the fluctuation-dissipation theorem that relates the dynamic structure factor to the dielectric function of the system. In a solid, due to the charge inhomogeneity, a concept of dielectric matrix $\varepsilon_{\mathbf{G},\mathbf{G}'}(\tilde{\mathbf{q}},\omega)$ has to be introduced. Here $\mathbf{G}$ and $\mathbf{G}'$ are reciprocal lattice vectors and $\tilde{\mathbf{q}}$ is restricted to the first Brillouin zone. In the

[3] This is, of course, the behavior observed already by Compton [1] and Debye [2].

random phase approximation (RPA) the dielectric matrix of a crystalline solid is given by [23, 24]

$$\begin{aligned}\varepsilon_{\mathbf{G},\mathbf{G}'}(\tilde{\mathbf{q}},\omega) &= \delta_{\mathbf{G},\mathbf{G}'} - \frac{4\pi}{|\tilde{\mathbf{q}}+\mathbf{G}|^2\Omega}\sum_{\mathbf{k}ij}\langle i\mathbf{k}|e^{-i(\tilde{\mathbf{q}}+\mathbf{G})\cdot\mathbf{r}}|j\tilde{\mathbf{k}}\rangle\langle j\tilde{\mathbf{k}}|e^{i(\tilde{\mathbf{q}}+\mathbf{G}')\cdot\mathbf{r}}|i\mathbf{k}\rangle \quad (11)\\ &\times \frac{n_f(E_{i\mathbf{k}})-n_f(E_{j\tilde{\mathbf{k}}})}{\omega+E_{i\mathbf{k}}-E_{j\tilde{\mathbf{k}}}+i\delta}\end{aligned}$$

where $|i\mathbf{k}\rangle$ is a single-particle state with a crystal momentum $\mathbf{k}$ and a band index i. Here $E_{i\mathbf{k}}$ is the band-energy and $n_f(E_{i\mathbf{k}})$ the corresponding occupation number. The momentum $\tilde{\mathbf{k}}$ is chosen so that the momentum conservation is fulfilled in the matrix elements. In normal NRIXS only the diagonal ($\mathbf{G}=\mathbf{G}'$) [25] elements of the inverse of the matrix $\varepsilon_{\mathbf{G},\mathbf{G}'}$ are needed and the dielectric function in the Eq. (7) is given by $\varepsilon_M(\mathbf{q},\omega) = 1/\varepsilon^{-1}_{0,0}(\mathbf{q},\omega)$, where $\mathbf{q}=\tilde{\mathbf{q}}+\mathbf{G}$ is the momentum transfer. The plasmon oscillation frequency is now defined by $\det\left[\varepsilon_{\mathbf{G},\mathbf{G}'}(\tilde{\mathbf{q}},\omega^{pl}(\tilde{\mathbf{q}}))\right] = 0$ [25]. The lowest order approximation for ε_M is to set it equal to $\varepsilon_{0,0}$ [26]

$$\begin{aligned}\varepsilon_M(\mathbf{q},\omega) &= 1 - \frac{4\pi}{|\mathbf{q}^2|\Omega}\sum_{\mathbf{k}ij}\langle i\mathbf{k}|e^{-i\mathbf{q}\cdot\mathbf{r}}|j\tilde{\mathbf{k}}\rangle\langle j\tilde{\mathbf{k}}|e^{i\mathbf{q}\cdot\mathbf{r}}|i\mathbf{k}\rangle \quad (12)\\ &\times \frac{n_f(E_{i\mathbf{k}})-n_f(E_{j\tilde{\mathbf{k}}})}{\omega+E_{i\mathbf{k}}-E_{j\tilde{\mathbf{k}}}+i\delta}.\end{aligned}$$

This is the lowest-order approximation for the full dielectric function that can give rise to plasmons with the familiar plasmon dispersion relation $\varepsilon_M(\mathbf{q},\omega^{pl}(\mathbf{q}))=0$. A solid responds to a disturbance with wave vector $\mathbf{q}$ at all the wave vectors $\mathbf{q}+\mathbf{G}$, where $\mathbf{G}$ is any reciprocal lattice vector. These are commonly called *local-field effects* and these effects are included in RPA but not in Eq. (12). This is the explanation for the difference between the two plasmon dispersion relations. However, the approximation given by Eq. (12) has been found to work relatively well for simple metals, but for semiconductors the local-field effects were found to be more important for small q [27].

3.2 Single-Particle Green's Function

The single-particle Green's function (G_1) describes an excitation of the system where a single particle is removed from an occupied state (hole added) or added to an unoccupied state. For non-interacting particles the single-particle Green's function G_1^0 is defined by

$$(i\frac{\partial}{\partial t_1} - \hat{H}_0)G_1^0(1,1') = \delta(1-1')$$

where $\hat{H}_0 = -\nabla_1^2/2m + V_{ext}(1)$ is the Hamiltonian operator with an external (crystal) potential. The indices $1, 1', \ldots$ represent the space ($\mathbf{r}_i$), the spin (σ_i) and the time

(t_i) coordinates. To go beyond the single-particle approximation a Dyson equation can be used

$$G_1(1,1') = G_1^0(1,1') + \int d(23)\, G_1^0(1,2)\Sigma(2,3)G_1(3,1'), \tag{13}$$

where Σ is the so-called self-energy and it describes the effects of the electron-electron interactions in the system. In solids Hedin's GW-approximation (GWA) [28] is often used to approximate the self-energy. In the GWA the self-energy of the electrons can be expressed as

$$\Sigma(1,1') = -i\delta(1,1') \int d2\, v(1,2)G_1(2,2^+) + iW(1^+,1')G_1(1,1') \tag{14}$$

where v is a bare Coulomb interaction and W is a screened one. W is given in terms of a dielectric function ε as

$$W(1,1') = \int d2\, v(1,2)\varepsilon^{-1}(2,1'). \tag{15}$$

In Eq. (14) the first term is the Hartree term and the second term represents the exchange and correlation. In principle the equations for the Green's function $G(\Sigma)$, the self-energy $\Sigma(G,W)$, and the screened interaction $W(G)$ should be solved self-consistently [29]. In the cases where this has been done [30] the fully self-consistent GW has been found to give poorer results than the non-self-consistent calculation (sometimes called G_0W_0). Calculations self-consistent with respect to G but not W (GW_0) gave more reasonable result but, for example, the jellium quasiparticle band widths were larger than the free electron result, in clear disagreement with the experimental results and G_0W_0 [31]. Additionally, the observed improvements were small and this is why the G_0W_0 approach is usually used [32].

Normally in solid state applications the GWA is transformed into a Dyson-type equation for the quasiparticle energies (E_m^{qp}) and states $|\phi_m^{qp}\rangle$ [29]

$$(\hat{H}_0 + \tilde{\Sigma}(E_m^{qp}))|\phi_m^{qp}\rangle = E_m^{qp}|\phi_m^{qp}\rangle, \tag{16}$$

which are solved self-consistently with respect to E_m^{qp}. These equations are either solved using local-density-approximation (LDA) [33] wave functions as basis set or assuming that the quasiparticle states are same as the LDA states. This approach to calculating the quasiparticle states and energies has been successfully applied to a wide range of electron systems [34]. Computationally the most extensive part of the calculation is the evaluation of the dielectric function in W. Although calculations including the full RPA dielectric function have been done, it is often more efficient to use a model dielectric function (see for example [35]). Usually when the results from the RPA approximation and these simpler approximations are compared the differences are small.

The self-energy has two types of effects on the dynamic structure factor. The real part of the self-energy changes the quasiparticle energies from the values predicted by mean-field theories. For example, in semiconductors this usually means that the center of gravity of the spectra will be moved to higher energies compared to the ones obtained, for example, by LDA. This effect is for the most part canceled by the electron-hole interaction which will be discussed in the next section. The imaginary part of the self-energy causes the quasiparticles to have a finite lifetime, i.e., the single-particle excitation can relax by coupling to the system. The lifetime effects are discussed in more detail in the last section of this thesis.

3.3 Electron-Hole Pairs

Inelastic x-ray scattering from an electron system creates an electron-hole pair excitation. The electron and the hole interact with the rest of the electrons in the system and this interaction turns into the self-energy discussed in the previous section. However, they also interact with each other, which should be included at the same level as their interaction with the rest of the system. This can be done consistently using so-called conserving approximations [36, 37] while calculating the two-particle Green's function. The effect of the electron-hole interaction for optical absorption was first studied by model calculations [38, 39]. Later also x-ray absorption was studied [40]. Recent *ab initio* calculations of optical absorption [41–45] including the electron-hole interaction have confirmed the importance of these effects in semiconductors and made possible a realistic comparison of calculated spectra with experiment. In this subsection the basic formalism for calculating two particle Green's functions is reviewed[4] and its application to NRIXS is presented later.

A two-particle Green's function (G_2) represents the excitation spectra of the system when two particles are added to it. For NRIXS the relevant two-particle Green's-function is one where a particle-hole pair is added to the system. A two-particle correlation function $L_2(1,2,1',2') = -G_2(1,2;1',2') + G_1(1,2)G_1(1',2')$ satisfies a *Bethe-Salpeter* equation (BSE)

$$L_2(1,2;1',2') = L_0(1,2;1',2') + \int d(3456)\, L_0(1,4;1',3)K(3,5;4,6)L_2(6,2;5,2'),$$

where $L_0(1,2;1',2') = G_1(1,2')G_1(1',2)$ is the two-particle correlation function of the non-interacting particle-hole pairs. The electron-hole interaction kernel K is given as a functional derivative of the self-energy [36]

$$K(3,5;4,6) = \frac{\delta\Sigma(3,4)}{\delta G_1(6,5)}.$$

This relation gives the "correct"(i.e. conserving) approximation of the electron-hole interaction kernel for a given approximation for the single-particle Green's function.

[4]This discussion follows closely the one in Refs. [40, 45], where also more details are given.

Using the GW-approximation for the self-energy and neglecting the derivative of the screened interaction with respect G_1 the result is

$$K(3,5;4,6) = -i\delta(3,4)\delta(5^-,6)v(3,6) + i\delta(3,6)\delta(4,5)W(3^+,4). \tag{17}$$

The first term is called *exchange* interaction (K_x) and it originates from the Hartree part of the self-energy. K_x is usually a repulsive interaction i.e. it shifts the spectral weight towards higher excitation energies. On the other hand, the screened interaction (K_d) is attractive (i.e., it shifts the spectra toward lower energies), and it is called *direct* term. K_d gives rise to what is often called the ladder-approximation.

The function L_2 depends on four independent time variables associated with the creation and annihilation times of the particles. When studying the response to an external perturbation and assuming an instantaneous creation and annihilation of the particle-hole pair there remain only two independent time variables [46]. Additionally, only the difference of these two times is relevant and one-dimensional Fourier-transformation with respect to time can be used to obtain a Lehmann representation for L. L_0 has a simple expression in energy space:

$$L_0(\mathbf{x}_1,\mathbf{x}_2,\mathbf{x}_1',\mathbf{x}_2';\omega) = i\sum_i^{occ}\sum_j^{unocc}\left[\frac{\psi_j(\mathbf{x}_1)\psi_i(\mathbf{x}_2)\psi_i^*(\mathbf{x}_1')\psi_j^*(\mathbf{x}_2')}{\omega-(E_j-E_i)} - \frac{\psi_i(\mathbf{x}_1)\psi_j(\mathbf{x}_2)\psi_j^*(\mathbf{x}_1')\psi_i^*(\mathbf{x}_2')}{\omega+(E_j-E_i)}\right]$$

where $\mathbf{x}_i = (\mathbf{r}_i,\sigma_i)$. The single quasiparticle energies are given by E_i and E_j and the corresponding states by ψ_i and ψ_j. Similar representation is obtained for L by assuming that the system has well-defined (i.e. long-lived) electron-hole excitations with energies Ω_λ and amplitudes

$$\chi_\lambda(\mathbf{x}_1,\mathbf{x}_2) = -\langle N,0|\psi^\dagger(\mathbf{x}_1)\psi(\mathbf{x}_2)|N,\lambda\rangle.$$

The expression for L in this basis is

$$L(\mathbf{x}_1,\mathbf{x}_2,\mathbf{x}_1',\mathbf{x}_2';\omega) = i\sum_\lambda\left[\frac{\chi_\lambda(\mathbf{x}_1,\mathbf{x}_{1'})\chi_\lambda^*(\mathbf{x}_{2'},\mathbf{x}_2)}{\omega-\Omega_\lambda} - \frac{\chi_\lambda^*(\mathbf{x}_{1'},\mathbf{x}_1)\chi_\lambda(\mathbf{x}_2,\mathbf{x}_{2'})}{\omega+\Omega_\lambda}\right].$$

In the modern solid state approaches BSE is transformed to a matrix problem by expanding the electron-hole wave function $\chi(\mathbf{x}_1,\mathbf{x}_2)$ in the basis of single-particle wave functions

$$\chi_\lambda(\mathbf{x}_1,\mathbf{x}_2) = \sum_i^{occ}\sum_j^{unocc}\left[A_{ij}^\lambda\psi_i^*(\mathbf{x}_2)\psi_j(\mathbf{x}_1) + B_{ij}^\lambda\psi_j^*(\mathbf{x}_2)\psi_i(\mathbf{x}_1)\right],$$

where coefficients A_{ij} represent the electron-hole pairs moving forward in time and B_{ij} those that move backward in time. The BSE reduces to a generalized matrix eigenvalue problem

$$(\mathbf{H}^0 + \mathbf{K}(\Omega_\lambda))\mathbf{v}_\lambda = \Omega_\lambda\mathbf{S}\mathbf{v}_\lambda, \tag{18}$$

where Ω_λ and $\mathbf{v}_\lambda = (\mathbf{A}^\lambda \mathbf{B}^\lambda)^T$ are the eigenvalue and the eigenstate coefficients, respectively. The matrix $\mathbf{S}$ can be expressed in terms of the identity matrix $\mathbf{1}$

$$\mathbf{S} = \begin{pmatrix} \mathbf{1} & \mathbf{0} \\ \mathbf{0} & -\mathbf{1} \end{pmatrix}.$$

$\mathbf{H}^0$ is the single-particle part of the Hamiltonian, and it is diagonal in the given basis i.e. $\mathbf{H}^0_{ij,i'j'} = \delta_{ij,i'j'}(E_j - E_i)$. The electron-hole interaction part of the Hamiltonian matrix $\mathbf{K}$ couples the different electron-hole pairs. The eigenvalue dependence of $\mathbf{K}$ is in the screened interaction.

In this work, instead of solving the full eigenvalue problem given in Eq. (18) the off-diagonal part of $\mathbf{K}$ coupling the backward and forward going pairs is neglected. In the language of Ref. [47] this means solving BSE within the Tamm-Dancoff approximation (TDA) instead of the RPA.[5] In the TDA the coefficients $\mathbf{A}$ and $\mathbf{B}$ can be solved separately and they result in the same excitations energies, different only in sign. In the cases where the influence of this non-diagonal part of $\mathbf{K}$ has been studied it has been found to have only a small effect on the resulting excitation energies Ω_λ [45]. Additionally, we only consider the spin-singlet electron-hole pairs and we neglect the eigenvalue dependence of $\mathbf{K}$. The resulting eigenvalue problem is

$$(E_j - E_i)A^\lambda_{ij} + \sum_{i'j'}[2K^x_{ij,i'j'} - K^d_{ij,i'j'}]A^\lambda_{i'j'} = \Omega_\lambda A^\lambda_{ij}, \tag{19}$$

where the exchange matrix elements $\mathbf{K}^x$ are

$$K^x_{ij,i'j'} = \int d\mathbf{r}d\mathbf{r}'\, \psi_i(\mathbf{r})\psi^*_j(\mathbf{r})v(\mathbf{r},\mathbf{r}')\psi^*_{i'}(\mathbf{r}')\psi_{j'}(\mathbf{r}'). \tag{20}$$

The coefficient in front of $\mathbf{K}^x$ in Eq. (19) comes from restricting the excitations to spin singlets. As mentioned, in the direct interaction, $\mathbf{K}^d$, the energy dependence of the screening is neglected ($W(\mathbf{r},\mathbf{r}',\omega) = W(\mathbf{r},\mathbf{r}',\omega = 0)$) and the matrix elements are

$$K^d_{ij,i'j'} = \int d\mathbf{r}d\mathbf{r}'\, \psi_i(\mathbf{r})\psi^*_j(\mathbf{r}')W(\mathbf{r},\mathbf{r}')\psi^*_{i'}(\mathbf{r})\psi_{j'}(\mathbf{r}'). \tag{21}$$

There are two advantages in approximating the full eigenvalue problem of Eq. (18) with Eq. (19). The first one is that we are now dealing with a Hermitian eigenvalue problem. Additionally, since we neglected the eigenvalue and energy dependence of the direct interaction we can use the matrix operator in Eq. (19) as an *effective* Hamiltonian (H_{eff}) for the electron-hole system. In the next two sections this effective Hamiltonian will be used to calculate NRIXS spectra.

[5] This should not be confused with the RPA discussed earlier in connection with the dielectric matrices.

4 Scattering from Valence Excitations

The computational approach to inelastic x-ray scattering from the valence electrons is presented in this section. The effective Hamiltonian introduced in the previous section is used to calculate the dynamic structure factor for the valence NRIXS. Full description of the scheme applied to optical absorption can be found in [41, 42] and to NRIXS in Paper I of this thesis. Here some details of the computational procedures and the nature of the electron-hole interaction kernel are reviewed. The different aspects of the electron-hole interaction are discussed in light of comparison with recent experimental results for cubic boron nitride (cBN) [48]. A connection is also made to some of the earlier approaches to valence NRIXS and their results are compared to those of the current scheme for cBN.

4.1 Computational Method

The approach used in this thesis to calculate the DSF is based on the fluctuation-dissipation theorem that relates it to the longitudinal dielectric function $\varepsilon_M(\mathbf{q},\omega)$. This dielectric function is the response of the system to the total macroscopic field i.e. it also includes the electric field induced in the system. Following the formalism presented in the previous section the dielectric function can be calculated using the effective Hamiltonian:

$$\varepsilon_M(\mathbf{q},\omega) = 1 - \frac{4\pi}{q^2}\left[\langle 0|\hat{\rho}_{\mathbf{q}}\frac{1}{\omega - \hat{H}_{eff} + i\eta}\hat{\rho}^{\dagger}_{\mathbf{q}}|0\rangle - \langle 0|\hat{\rho}_{-\mathbf{q}}\frac{1}{\omega + \hat{H}_{eff} + i\eta}\hat{\rho}^{\dagger}_{-\mathbf{q}}|0\rangle\right], \quad (22)$$

where $\hat{\rho}^{\dagger}_{\mathbf{q}}$ is the density-fluctuation operator

$$\rho^{\dagger}_{\mathbf{q}} = \sum_{vc\mathbf{k}} \langle c\mathbf{k}+\mathbf{q}|e^{i\mathbf{q}\cdot\mathbf{r}}|v\mathbf{k}\rangle \hat{a}^{\dagger}_{c\mathbf{k}+\mathbf{q}}\hat{a}_{v\mathbf{k}}. \quad (23)$$

The states here are the conduction band electron state $|c\mathbf{k}+\mathbf{q}\rangle$ and the valence band hole state $|v\mathbf{k}\rangle$. The electron-hole pair wave function for this problem is a superposition of the valence-hole and a conduction-band-electron pairs with a momentum difference equal to the momentum transfer:

$$\Psi_{\mathbf{q}}(\mathbf{r}_e,\mathbf{r}_h) = \sum_{vc\mathbf{k}} C_{vc\mathbf{k}}\psi^{*}_{v\mathbf{k}}(\mathbf{r}_h)\psi_{c\mathbf{k}+\mathbf{q}}(\mathbf{r}_e) \doteq \sum_{vc\mathbf{k}} C_{vc\mathbf{k}}|vc\mathbf{k}\rangle_{\mathbf{q}}. \quad (24)$$

The single-particle wave functions in Eq. (24) are calculated in plane wave basis using pseudopotentials [49] within the LDA [33]. The band energies for the diagonal part in $\hat{H}_{eff}$ are modified to agree with the calculated GW band structure. This modification is done using a linear parameterization of the GW-band energies E^{qp} as a function of the LDA-band energies E^{LDA},

$$\begin{aligned} E^{qp}_{v\mathbf{k}} &= (1+A_v)E^{LDA}_{v\mathbf{k}} + B_v \\ E^{qp}_{c\mathbf{k}} &= (1+A_c)E^{LDA}_{c\mathbf{k}} + B_c, \end{aligned}$$

where the coefficients $A_{v,c}$ and $B_{v,c}$ are determined so that the self-consistency in Eq. (16) is fulfilled. This was usually done, as well as possible, in the full Brillouin zone, using all of the valence bands and up to ten conduction bands. These coefficients were then applied to all of the bands used in the calculation of ε_M.

The exchange interaction in this formalism introduces the local-field effects into ε_M. The local-field effect here means the effect of the *microscopic* (i.e. unit cell scale) fields induced by the *macroscopic* external field. In the single particle approach discussed in the section 3.1 these were introduced because ε_M was related to the inverse of the dielectric matrix $\varepsilon_{\mathbf{G},\mathbf{G}'}$. Despite the dissimilarity of these approaches they introduce the same effect on ε_M. The exchange interaction in the basis given in Eq. (24) is [41, 42]

$$ {}_{\mathbf{q}}\langle vc\mathbf{k}|K_x|v'c'\mathbf{k}'\rangle_{\mathbf{q}} = \sum_{\mathbf{G}\neq\mathbf{0}} \frac{4\pi}{\Omega|\mathbf{q}+\mathbf{G}|^2}\rho^*_{\mathbf{G}}(v'c'\mathbf{k}')\rho_{\mathbf{G}}(vc\mathbf{k}). \tag{25} $$

The matrix elements $\rho_{\mathbf{G}}$ are calculated using Fourier transforms of the periodic parts $u_{n\mathbf{k}}$ of the band states (i.e. $\psi_{n\mathbf{k}}(\mathbf{r}) = e^{i\mathbf{k}\cdot\mathbf{r}}u_{n\mathbf{k}}(\mathbf{r})$):

$$ \rho_{\mathbf{G}}(vc\mathbf{k}) = \sum_{\mathbf{G}'} u^*_{c\mathbf{k}+\mathbf{q}}(\mathbf{G}')u_{v\mathbf{k}}(\mathbf{G}'-\mathbf{G}). $$

In the expression (25) for the exchange matrix elements the term $\mathbf{G}=\mathbf{0}$ is neglected. This is because the dielectric function ε_M represents the response of the system to the total field. If the term $\mathbf{G}=\mathbf{0}$ would be included the dielectric function in Eq. (22) would represent the response to the external field. This has been shown, for example, for exciton-type of wave functions by Cho et al. [50] and discussed in systems with general symmetry by Del Sole et al. [51].

The direct part of the electron-hole interaction is an approximation for the *local-field factor* mentioned in the introduction. Usually the local-field factor is approximated with a static one obtained from an electron gas approach (see for example [19]). Recently there have also been studies where time-dependent density-functional-theory [52] based approximation for the local-field factor has been used (see for example [13]). In the approach used in this work the direct part of the electron-hole interaction can be expressed as

$$ \begin{aligned} {}_q\langle vc\mathbf{k}|\hat{V}_d|v'c'\mathbf{k}'\rangle_q &= \sum_{\mathbf{R}}\int d\mathbf{x}d\mathbf{y}e^{i(\mathbf{k}'-\mathbf{k})\cdot(\mathbf{x}-\mathbf{y}+\mathbf{R})}u^*_{c,\mathbf{k}+\mathbf{q}}(\mathbf{x})u_{v,\mathbf{k}}(\mathbf{y})W(\mathbf{x}+\mathbf{R},\mathbf{y}) \\ &\times\ u_{c',\mathbf{k}'+\mathbf{q}}(\mathbf{x})u^*_{v',\mathbf{k}'}(\mathbf{y}), \end{aligned} \tag{26} $$

where the vectors $\mathbf{x}$ and $\mathbf{y}$ are restricted to an unit cell. The lattice vector $\mathbf{R}$ connects the unit cell where the hole ($\mathbf{y}$) is located to the one that the electron ($\mathbf{x}$) occupies. In this work the Hybertsen-Levine-Louie [35] approximation for the dielectric function in the screened interaction W is used. It is a generalized plasmon-pole approximation (GPPA) for the dielectric function and requires the dielectric constant ε_∞ of the solid.

The dielectric constant could, in principle, be calculated, for example, using the RPA, but the differences between using the RPA and the tabulated experimental values have only a small effect on the outcome of the calculation. This was demonstrated by Chang et al. [53], who also calculated the dielectric constant self-consistently for α-quartz and the result was in good agreement with the experimental value.[6] As explained in the paper I and Refs. [41, 42] the direct term is diagonal in the real-space representation of the particle-hole basis. Transforming the basis to the real space improves the computational efficiency of the method considerably because fast Fourier transform (FFT) techniques can be used.

The relative strength of the different parts of the electron-hole interaction depends on the material. In absorption the direct part has been found to be more important for semiconducting and insulating materials [42]. This has also been true for the DSF for the materials studied in this thesis. A similar conclusion, from quite a different starting point, has also been made in the case of aluminum [19], although it is not always true for metals (see for example [20]). In the next section the results for valence NRIXS in cubic boron nitrite (cBN) are calculated within different approximations. These are compared with the recent experimental results [48].

4.2 Application to cBN

In this subsection different approximations for the dynamic structure factor are compared in the case of cBN. The effects of using GW band energies with and without including the electron-hole interaction are looked at first. Next the effects of the different parts of the interaction are studied. Finally, the full calculation is compared with calculations using LDA band energies with and without the exchange contribution. Figure 1 shows the experimental results together with the calculated spectra with and without the electron hole interaction for cBN. The electron-hole interaction shifts the spectral features down by about 3 eV. Besides shifting the spectra, the electron-hole interaction also changes the relative weight and the shape of the spectral features. As an example, in the interacting calculation there is a double-peak structure at approximately 25 eV. This feature is not present in the calculation without the electron-hole interaction. In the next figure the relative importance of the different parts of the interaction is studied. In Fig. 2 the calculation with and without the exchange part of the interaction kernel are shown. It is clear that, at least for cBN, the direct part of the interaction is more important. The effect of $\mathbf{K}_x$ is to move the spectra to just slightly higher energies. As discussed in Ref. [45] the calculation with $\mathbf{K}_x = 0$ would be appropriate for the spin-triplet excitations.

[6] It should be noted here that Chang et al. used a RPA screening corrected for the exciton effects instead of the simple Hybertsen-Levine-Louie model used in this work.

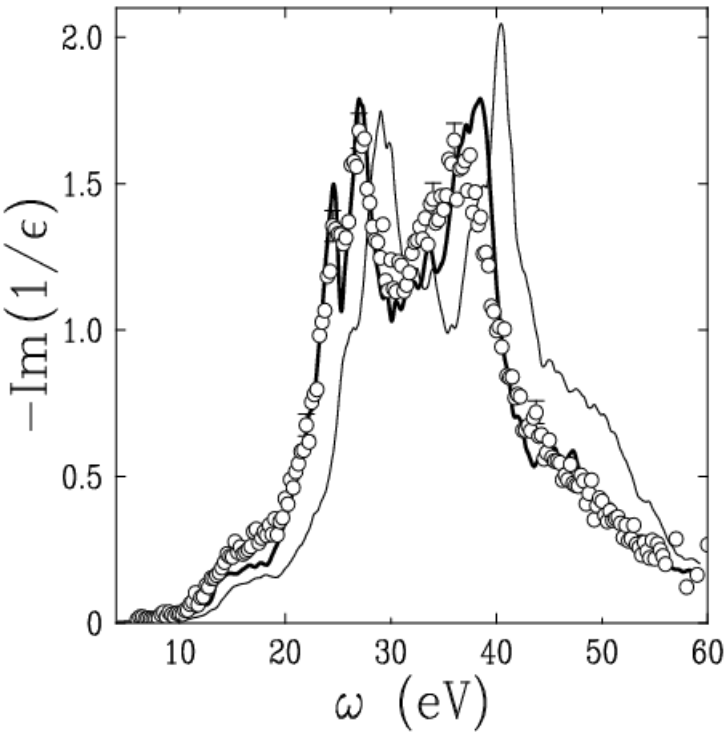

Figure 1: The experimental NRIXS spectrum together with two calculated spectra for cBN with momentum transfer 0.49 ΓX. The experimental spectrum (circles) and the spectra calculated using GW band energies with (bold solid line) and without (solid line) the electron-hole interaction are shown [48].

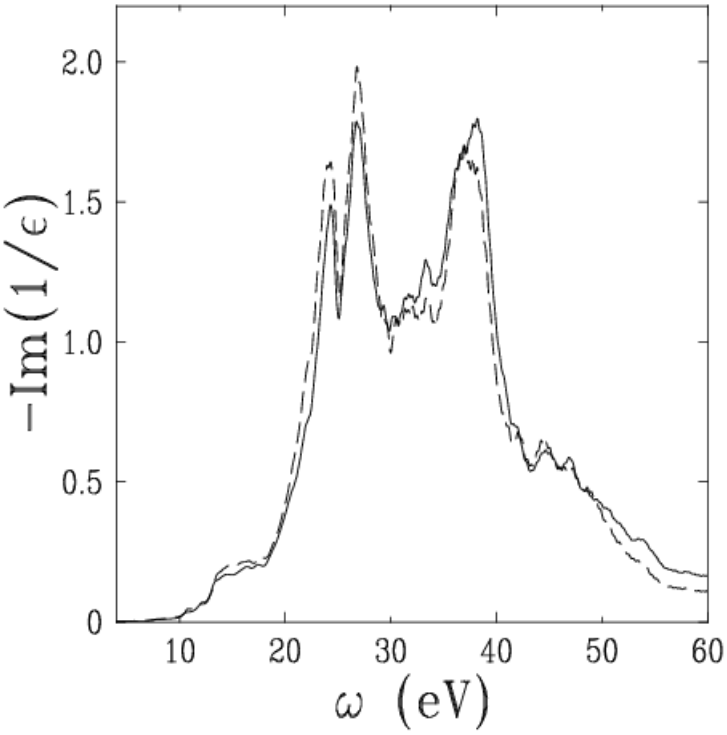

Figure 2: Two calculated spectra for cBN with the same momentum transfer as in Fig. 1. The spectra calculated using GW band energies with (solid line) and without (dashed line) the exchange part of the electron-hole interaction are shown.

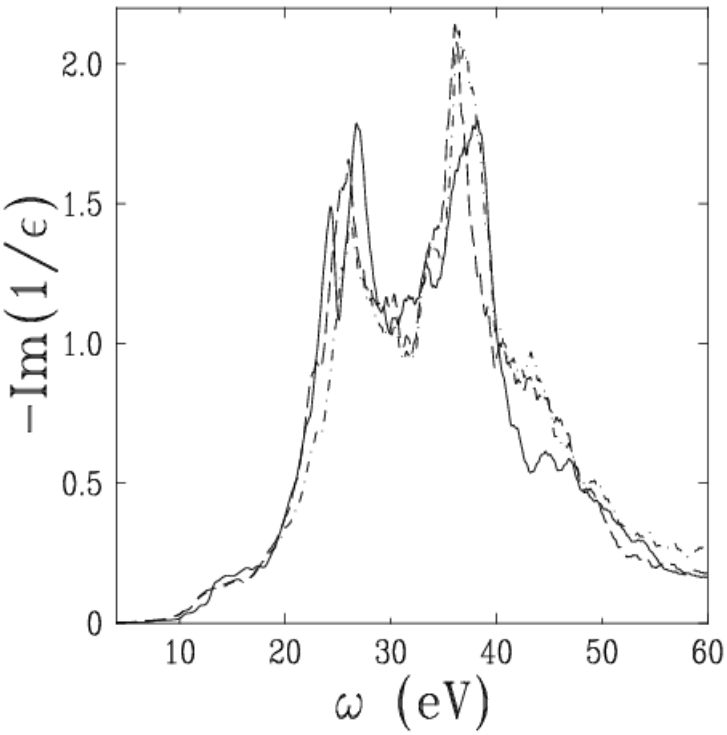

Figure 3: Three calculated spectra for cBN with the same momentum transfer as in Fig. 1. The spectrum calculated using *GW* band energies and with the electron-hole interaction is given by the solid line. The spectrum calculated with LDA band energies neglecting the local-field effects is given by the dashed line and the calculation with the local-field effects by the dash-dotted line.

To make a connection to earlier works on NRIXS a comparison with LDA-based approximations is also presented here. Figure 3 shows the result of the calculation based on the BSE with *GW* band energies (BSE+GW) and also two LDA calculations. The first approximation is to remove the electron-hole interaction from the effective Hamiltonian and use the LDA band energies. Additionally, the local-field effects are included by adding the exchange term into $\hat{H}_{eff}$. The comparison shows that, although the overall center of gravity of the spectrum is nearly the same in both LDA and BSE+GW, there still remains some differences in the details. For example, the relative weight of the dominating peaks in the spectra at 27 eV and 40 eV is closer to the experiment for the BSE+GW calculation than it is for either of the LDA based calculations. Additionally, the double-peak structure around 27 eV is not present at all in the LDA result. As before, the effect of including the exchange term or the local-field effects is rather small. In fact, the calculation without the exchange interaction and with the LDA band energies is closer to the experimental results than the approximation with $\mathbf{K}_x$.

5 Scattering from Core Excitations

In this section the non-resonant inelastic x-ray scattering from inner-shell excitations is discussed. X-ray absorption has attracted both experimental and theoretical interest since it can be applied, for example, to study the unoccupied states [54] and the structure of a system [55]. NRIXS could be used as an alternative technique to study these effects as has been demonstrated for several cases [56,57]. The approach used for core spectroscopy in this work is based on the Bethe-Salpeter formalism introduced in Section 3.3. The scheme is first reviewed and some unpublished details of the approach are presented. Again, the properties of core excitations are studied by comparing the calculated results with experimental ones. First the scattering from a core state in a wide-gap insulator is studied and the last part of this section is dedicated to the x-ray near edge structure in metals.

5.1 Computational Method

In this subsection a computational approach to NRIXS from the core excitations, also referred to as X-ray Raman Scattering (XRS), in solids is presented. The approach is based on the same method as the valence case with some exceptions. First of all the dynamic structure factor in this case is expressed as

$$S(\mathbf{q},\omega) = -\frac{1}{\pi}\mathrm{Im}\langle 0|\hat{\rho}_{\mathbf{q}}\frac{1}{\omega - \hat{H}_{eff} + i\eta}\hat{\rho}^{\dagger}_{\mathbf{q}}|0\rangle. \tag{27}$$

As before, the density fluctuation operator $\hat{\rho}_{\mathbf{q}}$ can be expressed in the second-quantized form given by Eq. (23). Since the core states studied in this work are tightly bound (or deep) core states, the electron-hole pair wave function can be expressed as

$$\Phi(\mathbf{r}_e,\mathbf{r}_h) = \sum_{n\mathbf{k}} C_{n\mathbf{k}}\psi_{n\mathbf{k}}(\mathbf{r}_e)[\psi^{TB}_{\mathbf{k}-\mathbf{q}\alpha}(\mathbf{r}_h)]^* \tag{28}$$

with $\psi_{n\mathbf{k}}(\mathbf{r}_e)$ being the conduction band wave function for the electron and $\psi^{TB}_{\mathbf{k}-\mathbf{q}\alpha}(\mathbf{r}_h)$ a tight-binding type expression for the core hole state. The index α represents the atomic quantum numbers nlm of the core hole and its position in the unit cell $\boldsymbol{\tau}$:

$$\psi^{TB}_{\mathbf{k}-\mathbf{q}\alpha}(\mathbf{r}_h) = \sum_{R} e^{i(\mathbf{k}-\mathbf{q})\cdot(\mathbf{R}+\boldsymbol{\tau})}\phi_{nlm}(\mathbf{r}_h - \mathbf{R} - \boldsymbol{\tau}). \tag{29}$$

An important approximation is made here, namely only the electron-hole pairs with the same nl numbers and same position $\boldsymbol{\tau}$ are included into the basis set given by Eq. (28). This means that the hole states are not allowed to move or relax to a different type of electron-hole pair. The effective Hamiltonian $\hat{H}_{eff}$ in Eq. (27) has an important difference when compared to the one used to calculate the dielectric function in Eq. (22). By comparing the definition of DSF in these two cases one can conclude that the $\mathbf{G} = 0$ term left out of $\mathbf{K}^x$ in the calculation of ε_M should

be included in Eq. (27). In other words, the DSF is the response to the external field [50]. An additional difference compared to valence excitations is that here the energy of the core hole is set to the measured value. In practice this means that for calculations the zero energy of the excitations is set equal to the conduction-band minimum. For comparison with the experimental results the calculated spectra are rigidly shifted to the same energy scale.

The conduction band states have been calculated using the pseudopotential plane-wave code. The matrix elements in the operators $\hat{\rho}_{\mathbf{q}}$ and $\mathbf{K}_x$ require calculating the overlap between the conduction band states and the core state. This is done with a pseudopotential-inversion scheme first introduced [58] and later refined [59] by Shirley et al. The current approach [59] is similar to the projector augmented wave (PAW) [60] method. In this approach the goal is to find an operator T that will reconstruct from a pseudo wave function $|\psi^{PS}\rangle$ the corresponding all electron (or true) wave function $|\psi^{AE}\rangle = T|\psi^{PS}\rangle$. The starting point of PAW is that every pseudo wave function can be expanded in terms of the pseudo partial waves $|\phi_i^{PS}\rangle$ in some augmentation region Ω_R close to a core:

$$|\psi^{PS}\rangle = \sum_i c_i |\phi_i^{PS}\rangle.$$

The corresponding all electron wave function would then be

$$|\psi^{AE}\rangle = T|\psi^{PS}\rangle = \sum_i c_i |\phi_i^{AE}\rangle \tag{30}$$

within Ω_R. In PAW the T is constructed by using projectors $|p_i\rangle$ that fulfill $\langle p_i|\phi_j^{PS}\rangle = \delta_{ij}$. From this it is easy to see that with $T = \sum_i |\phi_i^{AE}\rangle\langle p_i|$ the coefficient in Eq. (30) would be $c_i = \langle p_i|\psi^{PS}\rangle$. An additional requirement for the projectors is that they form a complete set in the sense that $\sum_i |\phi_i^{PS}\rangle\langle p_i| \approx \mathbf{1}$. In PAW the wave function can then be calculated everywhere in the crystal

$$|\psi^{AE}\rangle = T|\psi^{PS}\rangle = |\psi^{PS}\rangle + \sum_i c_i(|\phi_i^{AE}\rangle - |\phi_i^{PS}\rangle),$$

where the partial waves are only defined in the volume Ω_R. In this work we are interested in using this expansion close to the core where the core wave function ϕ_{nlm} is large, and this is why we only use the expansion as it is given in the Eq. (30). This expansion is accurate as long as the core state is limited to Ω_R. As said before, this method is used to calculate the matrix elements between the core state and the conduction band states. As an example, we write the matrix element needed for $\hat{\rho}_{\mathbf{q}}$ within the augmentation region Ω_R:

$$\begin{aligned} \langle \phi_{nlm}|e^{-i\mathbf{q}\cdot\mathbf{r}}|\phi_{n\mathbf{k}}\rangle &= \langle \phi_{nlm}|e^{-i\mathbf{q}\cdot\mathbf{r}}T|\phi_{n\mathbf{k}}^{PS}\rangle \\ &= \sum_i c_i^{n\mathbf{k}} \langle \phi_{nlm}|e^{-i\mathbf{q}\cdot\mathbf{r}}|\phi_i^{AE}\rangle, \end{aligned}$$

where $\phi_{n\mathbf{k}}$ denotes the partial wave of a conduction band state and the coefficients $c_i^{n\mathbf{k}}$ are obtained using the projectors. A similar, but a slightly more complicated formula can be obtained for the exchange matrix elements. In this work the projectors are calculated within the atomic code and tested on partial waves for a wide energy range.

The computation of the direct interaction $\mathbf{K}_d$ in XRS is complicated by the use of pseudopotential approach to the conduction band states. This means that the screening by the core and the valence electrons has to be considered separately. We break up the potential into three parts:

$$V_d(\mathbf{r}) = V_\alpha(\mathbf{r}) + \Delta V_\alpha(\mathbf{r}) + \Delta V_{val}(\mathbf{r}), \tag{31}$$

where $V_\alpha(\mathbf{r})$ is the bare core hole potential, $\Delta V_\alpha(\mathbf{r})$ accounts for the screening done by the core electrons (i.e., electrons that were included in the core when the pseudopotential was formed) and $\Delta V_{val}(\mathbf{r})$ for the screening by the valence electrons. The core screening is calculated within an atomic Hartree-Fock code and the valence screening is calculated as a response of the system to the potential $V_\alpha(\mathbf{r}) + \Delta V_\alpha(\mathbf{r})$:

$$\Delta V_{val}(\mathbf{r}) = \int d^3r' (\varepsilon^{-1}(\mathbf{r}, \mathbf{r}') - \delta(\mathbf{r} - \mathbf{r}'))(V_\alpha(\mathbf{r}') + \Delta V_\alpha(\mathbf{r}')). \tag{32}$$

The simple models, like GPPA [35], have been found to be inadequate and instead a calculation of RPA [61] static dielectric function $\varepsilon^{-1}(\mathbf{r}, \mathbf{r}')$ is required. Similarly the core screening potential should be the response to the potential $V_\alpha(\mathbf{r}) + \Delta V_{val}(\mathbf{r})$ and these equations (for $\Delta V_\alpha(\mathbf{r})$ and $\Delta V_{val}(\mathbf{r})$) should be solved self-consistently. Actually, in the cases it has been tested, the first iteration has been all that is needed.

The scheme presented here has been applied to XRS, x-ray absorption and electron energy loss spectroscopy for several materials. Here we present examples for XRS from F K edge in LiF [62] and K edge in Li-metal.

5.2 Application to F K edge in LiF

In this section the scheme is applied to XRS from $1s$ electrons of fluorine in lithium fluoride (LiF). LiF is a wide-gap insulator with strong excitonic effects both at the x-ray edge and in the valence spectra. The dispersion of the valence excitons has been studied both with NRIXS [63, 64] and with EELS [65, 66]. Also the momentum transfer dependence of the Li K edge exciton has attracted attention [63, 65]. The near edge x-ray absorption measurements of the fluorine K edge in LiF had strong peaks that were attributed to excitons [67]. Later calculations have confirmed these findings [68].

Here we study the momentum transfer dependence of the F K edge structure in LiF. The experimental spectra together with the calculated spectra for three momentum transfers can be found in Fig. 4. The spectra are normalized to have the same

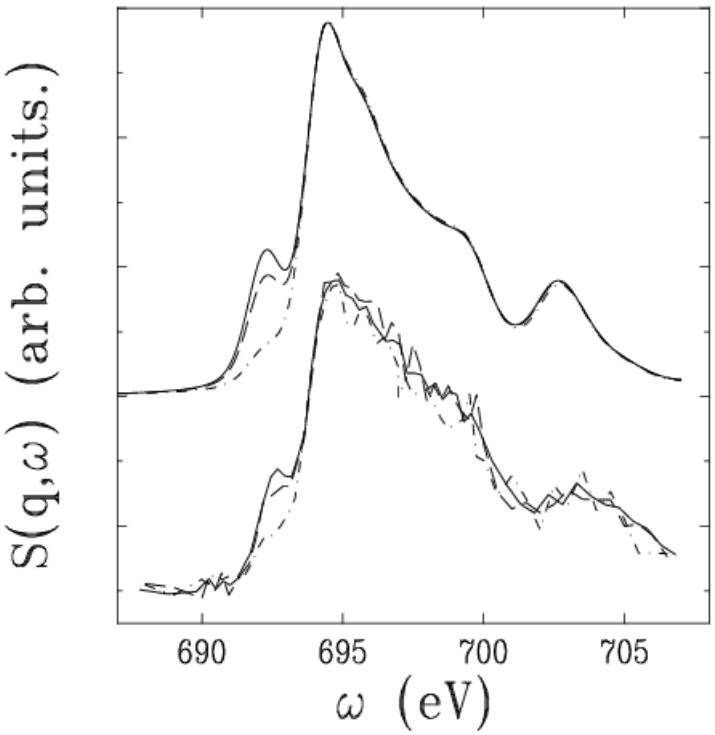

Figure 4: XRS results for F K edge in LiF. Three experimental spectra [62] with momentum transfers of 1.88 a.u. (dash-dotted line), 3.84 a.u. (dashed line), and 4.37 a.u. (solid line) are shown. Calculated results are offset for clarity.

area under the curve for the energy transfer above 695 eV. This was done to emphasize the momentum transfer dependence of the structure just below the edge. As can be seen from the figure, the structure below the edge becomes more pronounced compared to the other parts of the spectrum as the momentum transfer is increased. This can be explained by the fact that most of the scattering is due to dipole-allowed ($\Delta l = \pm 1$) transitions which behave as $S(\mathbf{q}, \omega) \propto q^2$. The theoretical calculations predict that the pre-peak structure is due to monopole transitions $\Delta l = 0$ and thus behave approximately as $S(\mathbf{q}, \omega) \propto q^4$. The position of the even-parity exciton with respect to the edge as well as its relative weight are quite accurately predicted by the current calculation. However, the near-edge odd-parity exciton's weight is slightly overestimated.

5.3 Application to K edge in Li metal

The x-ray near-edge structure of metals has attracted both theoretical and experimental interest. This is because the edge structure of metals can, at a qualitative level, be quite well predicted by the so-called Mahan-Nozieres-De Dominicis (MND) theory [69, 70]. The MND theory includes parameters that control the shape of the x-ray near edge structure and these parameters can, in principle, be determined from the experimental results. Various experimental methods have been used to estimate

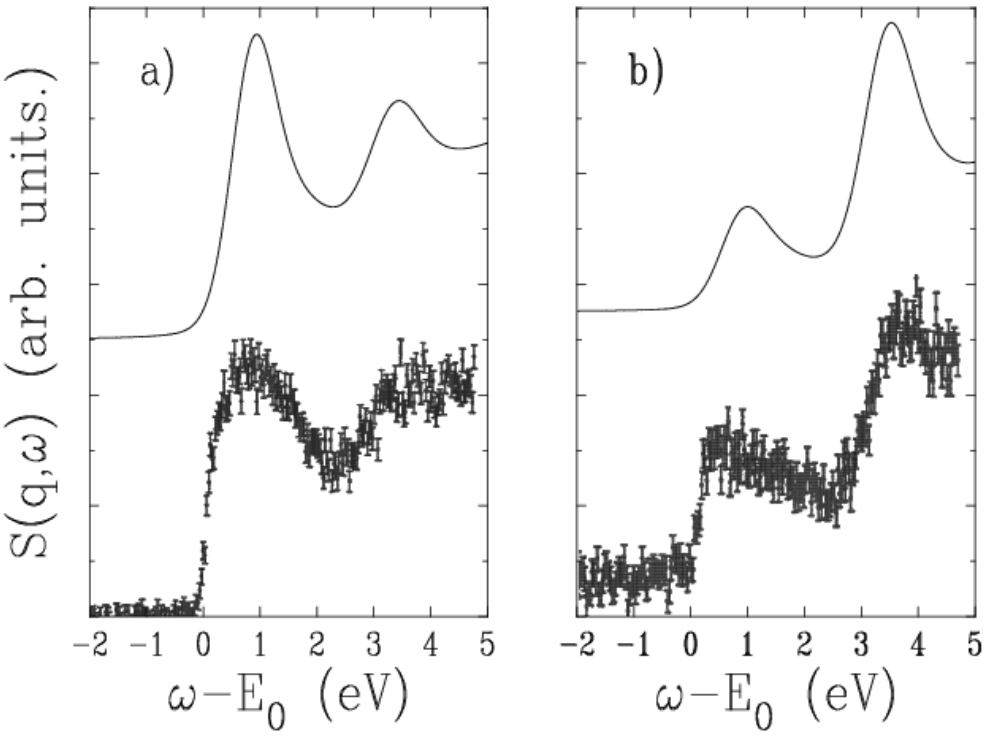

Figure 5: The experimental and the calculated spectra for XRS from the Li K edge in Li-metal. The experimental results are from Ref. [57]. The figure a) shows the result for the momentum transfer 0.46 a.u with the calculated spectra vertically shifted for clarity. b) same as a) but with 5.15 a.u. momentum transfer.

the value of these parameters. However, values obtained with different experimental methods can be quite different (some of the results for Li are given in [57]). This motivated Krisch et al. [57] to measure the momentum transfer dependence of the near K edge structure in Li metal. They were able to compare the fitted parameters for the monopole and dipole channels with previously obtained results. In Fig. 5 the experimental spectra [57] are shown together with the spectra calculated using the scheme presented in this thesis. The calculations correctly predict the shape and momentum-transfer-dependence of edge structure. Earlier experimental XRS spectra [56] on the Li K edge on a wider energy transfer range are given in Fig. 6. Again, the overall agreement between the calculation and the experiment is quite good. The spectral weight of the features above 65 eV is underestimated compared to the peak at the edge. Similar difference was found for the K edge in Be-metal studied in Paper III. The reason for this discrepancy has not been analyzed in detail in this work. However, one can speculate that either the screening of the core potential is underestimated in metals or the excitations that are responsible for this behavior cannot be represented in the particle-hole pair basis.

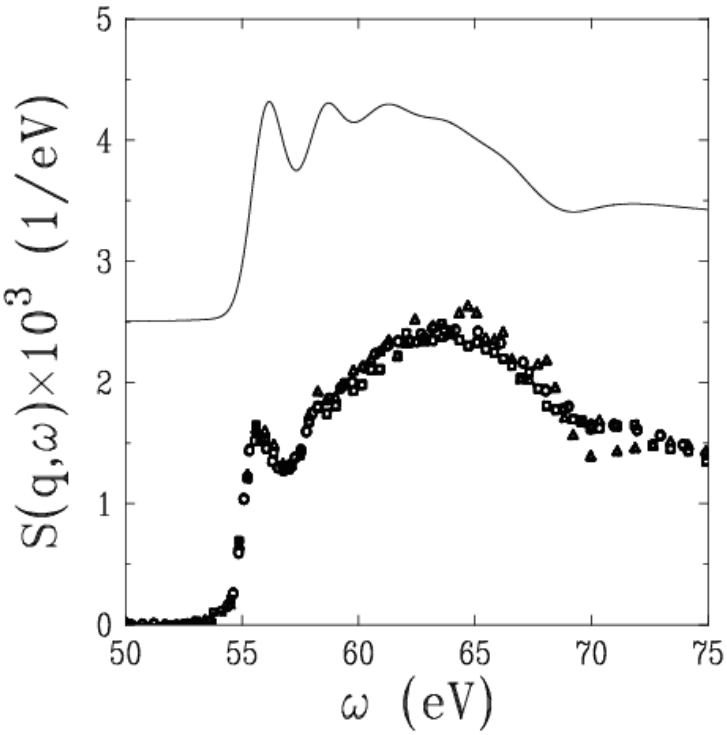

Figure 6: The experimental results [56] together with the calculation for the XRS from K edge in Li-metal. The momentum transfer is 0.93 a.u. and the experimental result for several directions of the momentum transfer is shown (see [56] for details). The calculated spectra for the Cartesian (100) direction is also shown.

6 Lifetime Effects and Non-resonant Inelastic X-ray Scattering

In this section we will discuss the effects of the electron-electron (or hole-electron) correlations on DSF that go beyond changing the single-particle energies. We do this by reviewing the properties of the electron self-energy and spectral function. First we will discuss how the damping or the lifetime broadening of the quasiparticle excitations can be seen in XRS spectra of metals. Next we will look into the effects of going beyond the quasiparticle picture. This will be done by introducing a formulation for the dynamic structure factor in the high-momentum-transfer region with the help of spectral functions. This will enable us to shed new light on the region of validity of the impulse approximation. The results in this section are mostly derived from the electron gas approximations for the self-energy in solids and they can only be considered to be qualitative. The damping of excitations in solids (including the crystal potential) has only been studied for excitations in range of few eV above the Fermi energy [71] and it is hard to use these results for XRS (excitation energies up to tens of eV are studied) or impossible to use them in Compton scattering (excitation energies in the order of at least hundreds of eV).

6.1 Lifetime Effects in Core Spectra

In the core spectra there are two corrections due to the imaginary part of the self-energy. The core hole has a finite lifetime because it can relax due to fluorescence or other processes such as Auger processes. All these processes can, as an approximation, be grouped together as a single energy- and momentum-transfer independent linewidth Γ_c. There is an additional damping due to the coupling of the excited electron with the other elementary excitations in the system. In this work this is included by using the on-shell[7] approximation to the imaginary part of the self-energy $\Sigma_2^e(\mathbf{p},\omega)$ of the final state electron. It is assumed that the final state electron momentum is determined by the energy of the excitations, i.e. $p(\omega) = \sqrt{2(\omega - E_0)}$, where E_0 is the binding energy of the core state. These effects are implemented by replacing the η in Eq. (27) by an energy-dependent damping $\Gamma(\omega) = \Gamma_c + |\Sigma_2^e(\mathbf{p}(\omega),\omega)|$:

$$S(\mathbf{q},\omega) = -1/\pi \mathrm{Im} \sum_{n\mathbf{k},n'\mathbf{k}'} \langle 0|\hat{\rho}_{\mathbf{q}}|n\mathbf{k}\alpha\rangle\langle n\mathbf{k}\alpha|(\omega - \hat{H} + i\Gamma(\omega))^{-1}|n'\mathbf{k}'\alpha\rangle\langle n'\mathbf{k}'\alpha|\hat{\rho}_{\mathbf{q}}^{\dagger}|0\rangle. \quad (33)$$

The fact that the on-shell approximation is used in this manner means that the Haydock recursion method [72] used in this thesis does not have to be modified.

As already pointed out, there has been many different approaches to the calculation of the electron self-energy. Here some of the simplest ones to implement are tested for approximating the electron lifetime effects in XRS. In Fig. 7 a) the XRS spectrum for energy transfer close to the Be K edge is given using two approximations for the self-energy and the corresponding on-shell self-energies are given in Fig. 7 b). The first of the self-energy approximations is the GWA calculated using generalized plasmon-pole approximation (GPPA) [35]. In the GPPA the self-energy is zero until the electron has enough energy (E_c) to excite a plasmon in the system. At E_c there is a sharp increase in the self-energy. In other words, in the GPPA there are no final state electron-lifetime effects in the spectra close to the edge and only for $\omega - E_0 > E_c$ the quasiparticle excitation has a finite lifetime. The other approximation is the electron gas GW self-energy calculated using Lindhard dielectric function (G_0W_0). In G_0W_0 there is also a contribution from exciting valence electron-hole pairs. This means that there are damping effects right from the edge of the spectra and a sharp increase due to the coupling with plasmons for excitation energy above $\tilde{E}_c$. The comparison in the Fig. 8 between the calculated spectra with G_0W_0 electron

[7] On-shell approximation here means that the imaginary part of the self-energy is only calculated on the energy shell,.i.e., by setting $\omega = p^2/2$ in the self-energy.

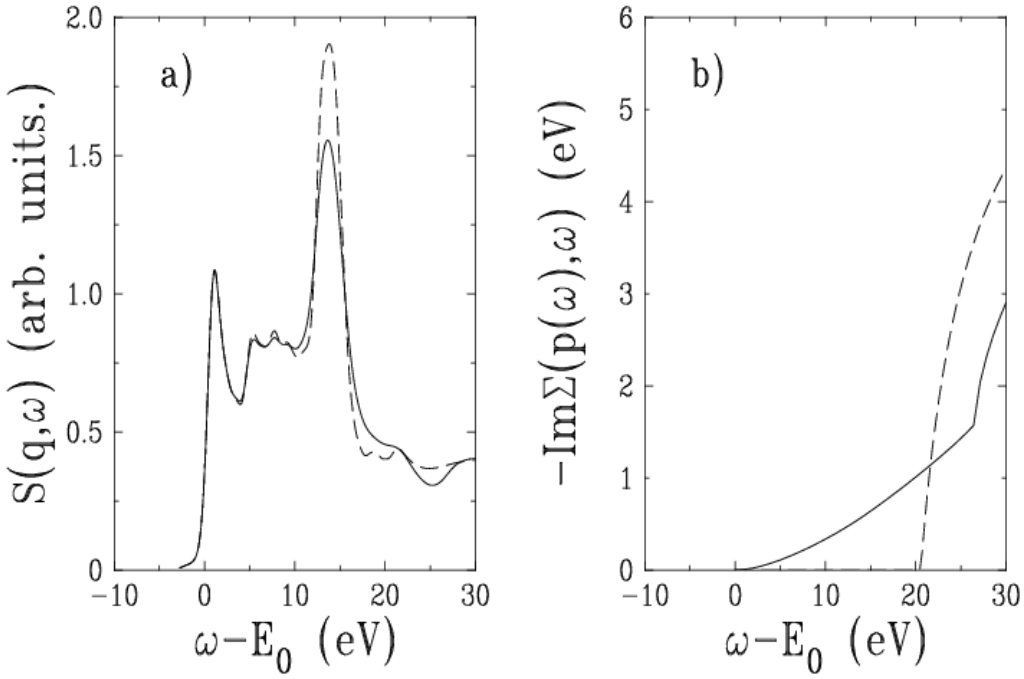

Figure 7: The effect of the final-state electron lifetime on Be K edge XRS spectra in Be-metal with momentum transfer of 1.25 a.u. along the c-axis. In a) the spectra calculated using G_0W_0 approximation (solid line) and GPPA (dashed line) for the final state electrons self-energy are shown. In b) the corresponding imaginary parts of the on-shell self-energies are shown.

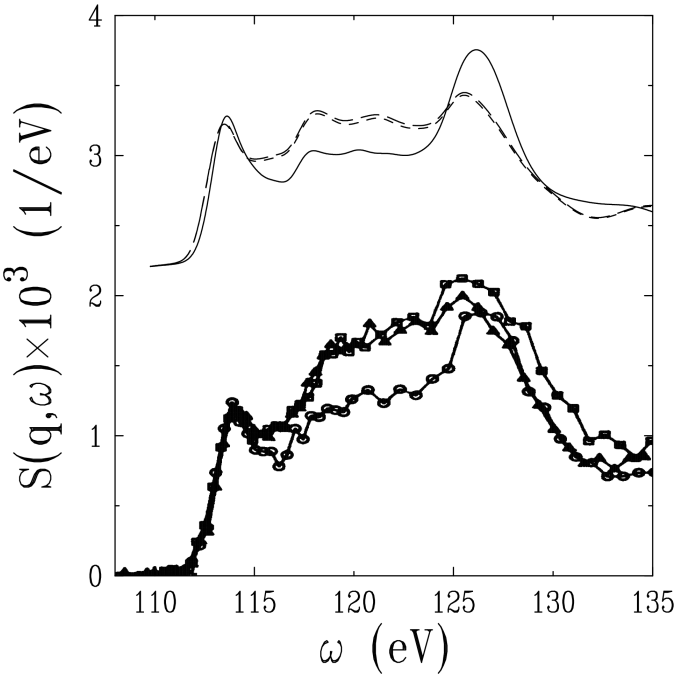

Figure 8: Experimental [56] and calculated XRS spectra for the K edge in Be metal for three directions. The magnitude of the momentum transfer vector is 1.25 a.u. and the experimental results for the momentum transfer along c-axis (circles), the [100]-direction (squares) and the [110]-direction (triangles) are shown. The corresponding calculated spectra, offset for clarity, are given by the solid, dashed and short dashed line, respectively.

self-energy effects and the experiment [56] shows the importance of correctly including these effects to the spectra. It also shows that the Lindhard approximation performs slightly better than the simpler GPPA. There is damping also below E_c and the damping is smaller above E_c than estimated by the GPPA.

6.2 Off-Shell Self-Energy Corrections to Impulse Approximation

The widely used impulse approximation is based on approximations about the final state of the electron system as well as the scattering process. The assumption about the scattering is that the energies of the initial state and the final state of the electron depend only on their respective momenta which are related by the momentum transfer. The other assumption is that the final state electron is a free and non-interacting particle. This enables one to approximate the dynamic structure factor with the simple formula given in Eq. (10). What is neglected in this picture is the interaction between the electron and the hole. Additionally the interaction of the final-state electron with the other electrons of the system is omitted. Most of the attempts to calculate corrections to the IA have concentrated on the electron-hole interaction [73,74]. Usually these approaches are applied to the core-electron Compton profile, for which the atomistic approach that they use is somewhat justified. The effects of the electron-electron interaction (or self-energy) on the IA are treated here with the approach discussed in paper V and in Ref. [75].

In the large-momentum-transfer regime the dynamic structure factor can be approximated by expressing it in terms of one particle spectral functions $A(\mathbf{k}, E) = 1/\pi|\mathrm{Im}G(\mathbf{k}, E)|$ [10]

$$S(\mathbf{q}, \omega) \approx \frac{2}{n} \int_{-\omega}^{0} d\omega' \int \frac{d\mathbf{p}}{(2\pi)^3} A(\mathbf{p}, \omega') A(\mathbf{p} + \mathbf{q}, \omega + \omega'). \tag{34}$$

The IA expression is obtained when: (i) in the second spectral function the energy ω' is replaced $p^2/2$ and (ii) the second spectral function is replaced by a delta function (free particle). This way one obtains the expression for IA approximation to DSF (as given in Eq. (10)). If only the approximation (i) is used the resulting expression for the DSF is

$$S(\mathbf{q}, \omega) \approx \int d\mathbf{p}\, \rho(\mathbf{p}) A(\mathbf{p} + \mathbf{q}, \omega + p^2/2). \tag{35}$$

Comparing this with Eq. (10) we can see that the effect of the spectral function is to act as a smoothing function. This effect was first pointed out in Ref. [76], where the main contribution to the on-shell self-energy was given. However, the on-shell result assumes that the final-state electron behaves as a well-defined quasiparticle. Within G_0W_0 the final-state spectral function has a double peak structure where the main peak is due to a quasiparticle excitation and the satellite peak is due to the coupling

of the electron with a plasmon. The role of the spectral function in Eq. (35) becomes more apparent if one realizes that the shape of spectral function changes quite slowly but its position follows closely the quasiparticle behavior. By presenting the spectral function on a shifted energy scale $\tilde{A}(k, E - k^2/2) = A(k, E)$ we obtain

$$S(\mathbf{q}, \omega) \approx \int d\mathbf{p}\, \rho(\mathbf{p}) \tilde{A}(\mathbf{p} + \mathbf{q}, \omega - \mathbf{p} \cdot \mathbf{q} - q^2/2). \tag{36}$$

Now it is possible to approximate $\mathbf{p} + \mathbf{q} \approx \mathbf{q}$ in $\tilde{A}$ and one obtains

$$S(\mathbf{q}, \omega) \approx \int d\omega'\, S^{IA}(\mathbf{q}, \omega') \tilde{A}(\mathbf{q}, \omega - \omega'), \tag{37}$$

where $S^{IA}(\mathbf{q}, \omega')$ is the usual IA result for $S(\mathbf{q}, \omega)$. From this it is easy to see that the final state electrons spectral function smears the experimental Compton profile. This smearing can explain much of the disagreement of the theoretical Compton profiles and the experimental ones for the high-resolution experiments (with the momentum transfer around 5 a.u.) [75]. However, a detailed study (paper V and Ref. [77]) of the momentum transfer dependence of this effect has shown that it is only a partial explanation of the observed differences. Still, this approximation is relatively easy to apply using the model spectral functions introduced in the paper V and should be used before the experimental result is compared to a theoretical Compton profile.

7 Summary of the Papers

The papers in this thesis give examples of how the final-state effects can be included in the description of non-resonant inelastic x-ray scattering. A number of computational methods are applied to this problem.

Paper *I* presents an *ab initio* scheme that was developed to study NRIXS from valence electrons in solids. It is an extension of a scheme that was developed earlier for optical absorption. It uses a Bethe-Salpeter equation approach to the correlation functions that has attracted much interest recently. The scheme is applied to non-resonant inelastic x-ray scattering from LiF, diamond and GaN.

Paper *II* presents results for both resonant inelastic x-ray scattering and non-resonant inelastic scattering. A scheme is presented here for resonant inelastic x-ray scattering and it is applied to cubic and hexagonal boron nitride. Also results for non-resonant scattering from Mg and O 1s electrons in MgO are presented.

Paper *III* presents an *ab initio* scheme to calculate the screening of the core hole potential and how it can be applied to core spectroscopy. Like paper *I* this work

also uses the Bethe-Salpeter equation as its starting point. The scheme is applied to NRIXS spectra for scattering from 1s electrons in Be metal. Additionally, it is applied to electron energy-loss scattering from Li 1s electrons in LiF, x-ray absorption near the F K edge in LiF and C K edge in diamond.

Paper *IV* presents results of the scheme of paper *III* applied to x-ray Raman scattering in several materials. The strongly bound exciton at the Be K edge in BeO is studied. Also the momentum-transfer-dependence of the Li K edge exciton structure is studied. Finally experimental and theoretical results for the C K edge in diamond are presented. The results are analyzed in the view of *ab initio* calculations.

Paper *V* is a qualitative study of the final-state electron self-energy and how it changes the range where impulse approximation is valid. An approximate formula for the final-state electrons self-energy and spectral function is presented.

8 Concluding Remarks

In this work the different aspects of the final-state interactions in non-resonant inelastic x-ray scattering were studied. Because of the large energy and momentum transfer range studied a variety of different approaches were used.

In the moderate-momentum-transfer region the scattering from valence excitations was studied using a two-particle Green's function scheme previously developed for optical absorption. What is new in this scheme, compared to most of the approaches to non-resonant inelastic x-ray scattering, is that the interaction between the excited electron and hole is taken into account at the *ab initio* level. This is why the method can be applied to study, for example, systems with strong valence exciton lines. However, the scheme is also quite reliable in systems where such excitations are not important. An interesting and challenging future development will be the application of this scheme to non-resonant inelastic x-ray scattering from metals.

The scattering from core-excited states was also studied using the two-particle Green's function method, although the approach was slightly modified from the one developed for the valence case due to the specific nature of core excited states. The detailed comparison of the experimental and calculated x-ray Raman scattering spectra showed that the scheme works reasonably well. The discovered differences will offer interesting possibilities for studying in more detail the properties of core excited states. Additionally, this scheme together with the one for valence excitations has been applied to resonant inelastic x-ray scattering, which still is a novel and rapidly growing application of the new synchrotron radiation sources. Again, this offers an invaluable opportunity for future research.

Additionally, the final-state lifetime broadening of both core and valence excited states was studied on a qualitative level using electron gas models for the self-energy. In the Compton regime these effects were found to explain much of the differences between the existing theories and experimental results. Since the results of this part of the thesis must be considered more qualitative, it will be interesting to see how more quantitative results, based on *ab initio* methods, will compare to the results presented here.

Other Work:

List of work by the author that is closely related to this thesis but not included in it.

1 W. A. Caliebe, **J. A. Soininen**, Eric L. Shirley, C.-C. Kao, and K. Hämäläinen, *Dynamic structure factor of diamond and LiF measured using inelastic x-ray scattering*, Phys. Rev. Lett. **84**, 3907 (2000).

2 K. Hämäläinen, S. Huotari, J. Laukkanen, **A. Soininen**, S. Manninen, C.-C. Kao, T. Buslabs, and M. Mezour, *Free electron gas under high pressure*, Phys. Rev. B **62** (Rapid Communications), R735 (2000).

3 C. Sternemann, K. Hämäläinen, A. Kaprolat, **A. Soininen**, G. Döring, C.-C. Kao, S. Manninen, and W. Schülke, *Final-state interaction in Compton scattering from electron liquids*, Phys. Rev. B **62** (Rapid Communication), R7687 (2000).

4 S. Galambosi, **J. A. Soininen**, K. Hämäläinen, Eric L. Shirley and C.-C. Kao *Non-resonant inelastic x-ray scattering study of cubic boron nitride*, editorially approved for publication in Phys. Rev. B.

5 S. Galambosi, **J. A. Soininen**, K. Hämäläinen, and Eric L. Shirley *Non-resonant inelastic x-ray scattering study of fluorine K-edge exciton in LiF*, to be submitted to Phys. Rev. B. (In May 2001).

References

[1] A. H. Compton, Phys. Rev. **21**, 207 and 483 (1923).

[2] P. Debye, Physikalische Zeitschrift **24**, 165 (1923).

[3] J. W. M. DuMond, Phys. Rev. **33**, 643 (1929).

[4] E. D. Isaacs and P. Platzman, Physics Today, February 1996, p. 40.

[5] for early work see P. Eisenberger, P. M. Platzman, and H. Winick, Phys. Rev. Lett. **36**, 623 (1976); P. Eisenberger, P. M. Platzman, and H. Winick, Phys. Rev. B **13**, 2377 (1976).

[6] example of recent work see K. Hämäläinen, J. P. Hill, S. Huotari, C.-C. Kao, L. E. Berman, A. Kotani, T. Idé, J. L. Peng, and R. L. Green, Phys. Rev. B **61**, 1836 (2000).

[7] *Compton Scattering*, edited by B. G. Williams (McGraw-Hill, New York 1977).

[8] P. Suortti, T. Buslaps, V. Honkimäki, C. Metz, A. Shukla, Th. Tschentscher, J. Kwiatkowska, F. Maniawski, A. Bansil, S. Kaprzyk, A. S. Kheifets, D. R. Lun, T. Sattler, J. R. Schneider, and F. Bell, J. Phys. Chem. Solids **61**, 397 (2000).

[9] Y. Sakurai, Y. Tanaka, A. Bansil, S. Kaprzyk, A. T. Stewart, Y. Nagashima, T. Hyodo, S. Nanao, H. Kawata, and N. Shiotani, Phys. Rev. Lett. **74**, 2252 (1995).

[10] W. Schülke, G. Stutz, F. Wohlert, and A. Kaprolat, Phys. Rev. B **54**, 14381 (1996).

[11] Y. Kubo, J. Phys. Soc. Jpn. **65**, 16 (1996); Y. Kubo, J. Phys. Soc. Jpn. **66**, 2236 (1997).

[12] W. Schülke, J. Phys. Soc. Jpn. **68**, 2470 (1999).

[13] A. G. Eguiluz, W. Ku, and J. M. Sullivan, J. Phys. Chem. Solids **61**, 383 (2000).

[14] L. Dobrzyński, J. Phys: Condens. Matter **12**, 87 (2000).

[15] S. B. Dugdale and T. Jarlborg, Solid State Commun. **105**, 283 (1998).

[16] C. Filippi and D. M. Ceperley, Phys. Rev. B **59**, 7907 (1999).

[17] W. Schülke, K. Höppner, and A. Kaprolat, Phys. Rev. B **54**, 17464 (1996); J. P. Hill, C.-C. Kao, W. A. Caliebe, D. Gibbs, and J. B. Hastings, Phys. Rev. Lett. **77**, 3665 (1996).

[18] N. E. Maddocks, R. W. Godby, and R. J. Needs, Phys. Rev. B **49**, 8502 (1994); A. Fleszar, A. A. Quong, and A. G. Eguiluz, Phys. Rev. Lett. **74**, 590 (1995); H. Bross and M. Ehrnsperger, Z. Phys. B **97**, 17 (1995).

[19] B. C. Larson, J. Z. Tischler, E. D. Isaacs, P. Zschack, A. Fleszar, and A. G. Eguiluz, Phys. Rev. Lett. **77**, 1346 (1996).

[20] A. Fleszar, R. Stumpf, and A. G. Eguiluz, Phys. Rev. B **55**, 2068 (1997).

[21] W. Schülke, *Handbook of Synchrotron Radiation* Vol. 3, 565, edited by G. S. Brown and D. E. Moncton, (North-Holland, Amsterdam 1991).

[22] L. Van Hove, Phys. Rev. **95**, 249 (1954).

[23] S. L. Adler, Phys. Rev. **126**, 413 (1962).

[24] N. Wiser, Phys. Rev. **129**, 62 (1963).

[25] W. M. Saslow and G. F. Reiter, Phys. Rev. B **7**, 2995 (1973).

[26] H. Ehrenreich and M. H. Cohen, Phys. Rev. **115**, 786 (1959).

[27] K. Sturm, Adv. Phys. **31**, 1 (1982).

[28] L. Hedin, Phys. Rev. **139**, A796 (1965).

[29] L. Hedin and S. Lundqvist, in *Solid State Physics, Advances in Research and Application*, edited by F. Seitz, D. D. Turnbull and H. Ehrenreich, (Academic, New York, 1969), Vol. 23, p. 1.

[30] B. Holm and U. von Barth, Phys. Rev. B **57**, 2108 (1998); W.-D. Schöne and A. G. Eguiluz, Phys. Rev. Lett. **81**, 1662 (1998).

[31] U. von Barth and B. Holm, Phys. Rev. B **54**, 8411 (1996); E. L. Shirley, Phys. Rev. B **54**, 7758 (1996).

[32] L. Hedin, J. Phys: Condens. Matter **11**, R489 (1999).

[33] P. Hohenberg and W. Kohn, Phys. Rev. **136**, B864 (1964); W. Kohn and L. J. Sham, Phys. Rev. **140**, A1133 (1965).

[34] see B. Arnaud and M. Alouani, Phys. Rev. B **62**, 4464 (2000) and references therein.

[35] Z. H. Levine and S. G. Louie, Phys. Rev. B **25**, 6310 (1982); M. S. Hybertsen and S. G. Louie, Phys. Rev. B **37**, 2733 (1988).

[36] G. Baym and L. P. Kadanoff, Phys. Rev. **124**, 287 (1961).

[37] L. P. Kadanoff and G. Baym, *Quantum Statistical Mechanics* (W.A. Benjamin Inc, New York 1962).

[38] L. J. Sham and T. M. Rice, Phys. Rev. **144**, 708 (1966).

[39] W. Hanke and L. J. Sham, Phys. Rev. Lett **43**, 387 (1979); W. Hanke and L. J. Sham, Phys. Rev. B **21**, 4656 (1980).

[40] G. Strinati, Phys. Rev. Lett. **49**, 1519 (1982); G. Strinati, Phys. Rev. B **29**, 5718 (1984).

[41] L. X. Benedict, E. L. Shirley, and R. B. Bohn, Phys. Rev. B **57**, R9385 (1998); L. X. Benedict, E. L. Shirley, and R. B. Bohn, Phys. Rev. Lett. **80**, 4514 (1998).

[42] L. X. Benedict and E. L. Shirley, Phys. Rev. B **59**, 5441 (1999).

[43] M. Rohlfing and S. G. Louie, Phys. Rev. Lett. **80**, 3320 (1998); M. Rohlfing and S. G. Louie, Phys. Rev. Lett. **81**, 2312 (1998).

[44] S. Albrecht, L. Reining, R. Del Sole, and G. Onida, Phys. Rev. Lett. **80**, 4510 (1998).

[45] M. Rohlfing and S. G. Louie, Phys. Rev. B **62**, 4927 (2000).

[46] P. Nozières, *Theory of Interacting Fermi Systems* (W.A. Benjamin Inc, New York 1964).

[47] See for example A. Fetter and J.D. Walecka, *Quantum Theory of Many Particle Systems* (McGraw-Hill Book Company, San Francisco, 1971), pp. 538-539.

[48] S. Galambosi, J. A. Soininen, K. Hämäläinen, Eric L. Shirley and C.-C. Kao, unpublished.

[49] For a review, see W. E. Pickett, Comput. Phys. Rep. **9**, 115 (1989).

[50] K. Cho, Solid State Commun. **33**, 911 (1980); K. Ehara and K. Cho, Solid State Commun. **44**, 453 (1982).

[51] R. Del Sole and E. Fiorino, Phys. Rev. B **29**, 4631 (1984).

[52] E. Runge and E. K. U. Gross, Phys. Rev. Lett. **52**, 997 (1984).

[53] E. K. Chang, M. Rohlfing, and S. G. Louie, Phys. Rev. Lett. **85**, 2613 (2000).

[54] J. Stöhr, *NEXAFS spectroscopy* (Springer, New York, 1992).

[55] *X-Ray Absorption: Principles, Applications, Techniques of EXAFS, SEXAFS and XANES*, editors D. C. Koningsberger and R. Prins (Wiley, New York, 1988).

[56] H. Nagasawa, S. Mourikis, and W. Schülke, J. Phys. Soc. Jpn. **58**, 710 (1989).

[57] M. H. Krisch, F. Sette, C. Masciovecchio, and R. Verbeni, Phys. Rev. Lett. **78**, 2843 (1997).

[58] E. L. Shirley, J. El. Spect. & Rel. Phenom. **110-111**, 305 (2000).

[59] E. L. Shirley, S. I. Merritt, and J. A. Soininen, unpublished.

[60] P. E. Blöchl, Phys. Rev. B **50**, 17953 (1994).

[61] M. S. Hybertsen and S. G. Louie, Phys. Rev. B **35**, 5585 (1987).

[62] S. Galambosi, J. A. Soininen, K. Hämäläinen, and Eric L. Shirley, unpublished.

[63] W.A. Caliebe, Ph.D. thesis, University of Kiel (1997).

[64] W. A. Caliebe, J. A. Soininen, E. L. Shirley, C.-C. Kao, and K. Hämäläinen, Phys. Rev. Lett. **84**, 3907 (2000).

[65] J. R. Fields, P. C. Gibbons, and S. E. Schnatterly, Phys. Rev. Lett. **38**, 430 (1977).

[66] A. A. Cafolla, Ph.D. thesis, University of Virginia (1985).

[67] E. Hudson, E. Moler, Y. Zheng, S. Kellar, P. Heimann, Z. Hussain, and D. A. Shirley, Phys. Rev. B **49**, 3701 (1994).

[68] E. L. Shirley, Phys. Rev. Lett. **80**, 794 (1998).

[69] G. D. Mahan, Phys. Rev. **163**, 612 (1967).

[70] P. Nozières and C. T. De Dominicis, Phys. Rev. **178**, 1097 (1969).

[71] I. Campillo, J. M. Pitarke, A. Rubio, E. Zarate, and P. M. Echenique, Phys. Rev. Lett. **83**, 2230 (1999); I. Campillo, J. M. Pitarke, A. Rubio, and P. M. Echenique, Phys. Rev. B. **62**, 1500 (2000).

[72] R. Haydock, in *Solid State Physics*, edited by H. Ehrenreich, F. Seitz, and D. D. Turnbull, (Academic, New York, 1980), Vol. 35, p. 215.

[73] A. Issolah, B. Lèvy, A. Beswick, and G. Loupias, Phys. Rev. A **38**, 4509 (1988); A. Issolah, Y. Garreau, B. Lèvy, and G. Loupias, Phys. Rev. B **44**, 11029 (1991).

[74] P. Holm and R. Ribberfors, Phys. Rev. A **40**, 6251 (1989).

[75] C. Sternemann, K. Hämäläinen, A. Kaprolat, A. Soininen, G. Döring, C.-C. Kao, S. Manninen, and W. Schülke, Phys. Rev. B **62**, R7687 (2000).

[76] B. I. Lundqvist and C. Lyden, Phys. Rev. B **4**, 3360 (1971).

[77] C. Sternemann, private communication.